Lateral Ordering of Cylindrical Microdomains Under Solvent Vapor

Soojin Park,[†] Bokyung Kim,[†] Ji Xu,[†] Tommy Hofmann,[‡] Benjamin M. Ocko,[‡] and Thomas P. Russell*,[†]

Department of Polymer Science and Engineering, University of Massachusetts, Amherst, Massachusetts 01003, and Department of Physics, Brookhaven National Laboratory, Upton, New York 11973

Received July 17, 2008

ABSTRACT: The development of the morphology in asymmetric polystyrene-*block*-poly(4-vinylpyridine) (PS-*b*-P4VP) thin films in tetrahydrofuran (THF) vapor, a selective solvent for majority PS block, as a function of time was investigated by scanning force microscopy (SFM) and grazing incidence small-angle X-ray scattering (GISAXS). When the PS-*b*-P4VP films were spin-coated from a toluene/THF mixture onto a silicon substrate, cylindrical microdomains were found to be oriented normal to the surface. By annealing under the THF solvent vapor, the distribution of the size and center-to-center distance between the cylindrical microdomains were significantly narrowed. The orientation and grain size of the cylindrical microdomains in the annealed films were characterized using Moiré analysis obtained from SFM scan. GISAXS was used to characterize the morphology of the entire film.

Introduction

Block copolymers (BCPs) consist of two or more chemically different polymer chains covalently joined at one end.[1−6] Nonfavorable interactions between the segments in the blocks result in a microphase separation of the BCP into periodic arrays of spherical, cylindrical, or lamellar microdomains, depending on the volume fraction of the blocks, that are tens of nanometers in size. BCPs are of increasing interest because in thin films the oriented ordered arrays of these microdomains are ideal templates and scaffolds for the fabrication of nanostructured materials.[7−10] BCP templates are finding use as polarizer,[11] templates for microelectronic integrated circuits,[12] magnetic media,[13] and optical waveguides.[14,15] The key in the use of BCPs is the control over the orientation and lateral ordering of the microdomains in thin films. In recent years, a number of approaches have been developed to control the orientation and enhance the lateral order of microdomains by applying external fields, like electric fields,[16] shear,[17] temperature gradients,[18] graphoepitaxy,[19] chemically patterned substrates,[20] controlled interfacial interactions,[21,22] zone casting,[23] optical alignment,[24] and solvent fields.[25−32]

Because solvent can escape from a film only at the surface, solvent evaporation is a strong, highly directional field. In addition, the concentration of solvent normal to the film surface is not uniform, but rather, there is a gradient of the solvent concentration, with the solvent concentration being lowest at the surface and highest in the interior of the film. With time, as solvent evaporates, this gradient solvent field propagates into the film until the solvent has evaporated. The presence of a solvent in a block copolymer films performs several important functions, when the orientation and lateral ordering of the microdomains is of interest. First, the solvent mediates surface energies and, hence, tends to orient the microdomains normal to the surface, as long as there is no strong preferential interaction of the solvent with one of the blocks. If this is the case, the solvent will tend to orient the microdomains parallel to the surface. Second, the copolymer in solution is dissolved with no ordering while, in the solid state, the BCP microphase separates. Consequently, the gradient in the solvent concentration corresponds to a gradient in the ordering of the BCP with microphase separation occurring initially at the film surface first. As the solvent evaporates, subsequent microphase separation of the BCP is templated by the ordered structure at the surface of the film. Third, the presence of the solvent imparts significant mobility to the BCP, markedly reducing the glass transition temperature.[33] Consequently, the grains of the microdomains formed initially can rapidly coarsen. Therefore, during the evaporation of solvent, multiple processes are occurring simultaneously and the resultant order and orientation of the BCP thin film will depend upon a balance of the kinetics associated with each. With this in mind, it should be noted that the morphology of the film generated by solvent casting or solvent annealing is, in general, far removed from the equilibrium morphology of the BCP, which is dictated by the surface energies of each block, the interactions of each block with the substrate, and the commensurability between the film thickness and the equilibrium period of the BCP in the bulk. By thermally annealing a spin-coated BCP film for sufficient time, the morphology will, in general, reach an equilibrium morphology subject to the constraints placed on the morphology.

Kim et al. first reported that solvent evaporation could be used to induce the ordering and orientation of BCP microdomains.[25] Vertically aligned cylindrical PS microdomains could be obtained in a polystyrene-*block*-polybutadiene-*block*-polystyrene triblock copolymer thin films with a thickness of ∼100 nm. The same effect was also observed in a polystyrene-*block*-poly(ethylene oxide) (PS-*b*-PEO) and polystyrene-*block*-poly(L-lactide) BCP thin films and was attributed to a copolymer/solvent concentration gradient normal to the film surface as discussed above.[26,27] This orientation was found to be independent of the substrate. However, the lateral ordering of the cylindrical microdomains was poor. Hahm et al. and, later, Kimura et al. showed that evaporation-induced flow, in solvent cast BCP films, produced arrays of nanoscopic cylinders oriented normal to the surface with a high degree of ordering.[28,29] Recently, Ludwigs et al. demonstrated that solvent annealing could markedly enhance the ordering of BCP microdomains in thin films.[30] By controlling the rate of solvent evaporation and solvent annealing in thin films of PS-*b*-PEO, Kim et al. achieved nearly defect-free arrays of cylindrical microdomains oriented normal to the film surface that spanned from the surface to the substrate.[31] Moreover, the use of a cosolvent enabled further control over the length scale of lateral ordering. More recent

* To whom correspondence should be addressed. Tel.: 1-413-545-2680. Fax: 1-413-577-1510. E-mail: russell@mail.pse.umass.edu.
[†] University of Massachusetts.
[‡] Brookhaven National Laboratory.

10.1021/ma802480s CCC: $40.75
Published on Web 01/28/2009

results showed that cylindrical microdomains oriented normal to the film surface could be obtained directly by spin-coating polystyrene-*block*-poly(4-vinylpyridine) (PS-*b*-P4VP) BCPs from mixed solvents of toluene and tetrahydrofuran (THF) and arrays of highly ordered cylindrical microdomains formed over large areas after exposing the films to vapor of a toluene/THF mixture. This process was independent of substrate, but strongly dependent on the quality of the solvents for each block and the solvent evaporation rate.[34]

In this work, the time evolution of cylindrical microdomains oriented normal to the surface under solvent vapor and the degree of swelling in thin films as a function of annealing time was investigated. As solvent annealing time increased, the distribution of the microdomain size and the interdomain distance between the cylindrical microdomains significantly decreased and the lateral order of cylindrical microdomains was greatly enhanced. Even though THF is a slightly selective solvent for the major component block, the cylindrical microdomains oriented normal to the film surface and reached a morphology that did not change with further annealing time. Over large areas, the films were characterized using a Moiré interference pattern analysis and grazing incidence small-angle X-ray scattering (GISAXS). After solvent annealing in THF vapor for 4 h, cylindrical microdomains oriented normal to the film surface were obtained with a single grain of at least 10 × 10 μm^2 in size. The methods mentioned above offer useful tools for characterization of BCP microdomains in thin films over large areas.

Experimental Section

Materials. PS-*b*-P4VP diblock copolymer was purchased from Polymer Source and was used without further purification. The block copolymers were characterized with size exclusion chromatography (SEC) and nuclear magnetic resonance (^{1}H NMR) spectroscopy. The number average molecular weight of PS-*b*-P4VP and weight fraction of PS are 70.2 kg/mol and 0.70, respectively. The polydispersity is 1.11. For the SEC analysis, two PS gel columns (Polymer Laboratory., PL-mixed C, 300 mm × 80 mm) were used and the eluent was *N*,*N*-dimethylformamide (DMF, Fisher, HPLC grade). The temperature of the column was kept at 40 °C using a column oven (Eppendorf, TC-50). Chromatograms were recorded with a multiangle laser light scattering detector (Wyatt, mini-DAWN) and a refractive index detector (Wyatt, Opti-Laboratory). The dn/dc value of PS-*b*-P4VP in DMF was measured as 0.135 mL/g by a refractive index detector. PS-*b*-PVP copolymers were dissolved in toluene/THF solvent mixtures (70/30, v/v) at 70 °C for 2 h and cooled to room temperature to yield a 1 wt % polymer solution. Toluene and THF were of analysis grade (Fisher). PS-*b*-PVP thin films were fabricated by spin-coating typically at 3000 rpm and 60 s from a 1 wt % toluene/THF solution on the silicon substrate (International Wafer Service, Inc.) cleaned with oxygen plasma.

Characterization of Morphology in Thin Films. Spin-coated films were exposed to pure THF vapor for 0.5−4 h to induce mobility and allow microphase separation to occur under N_2. To control the solvent vapor treatment process, the samples were kept at a constant temperature (23 °C) in a small vessel with the vapor saturated with solvent (bubbled through a solvent reservoir) as schematically shown in Figure 1. The concentration of solvent in the chamber was used at fixed flow rates (0.1 mL/min) of solvent infused nitrogen. An interferometer (Filmetrics F20) was used to measure the thickness of the film during solvent annealing. Solvent was removed from the film by passing pure nitrogen through the chamber, and the sample was dried further in vacuum for 2 h. When the solvent annealed films were immersed in ethanol for 20 min, nanoporous structure can be generated without changing the separation distance and size of circular domains. The surface topography of PS-*b*-P4VP thin films on a silicon wafer was imaged by scanning force microscope (Digital Instruments, Multiple-mode

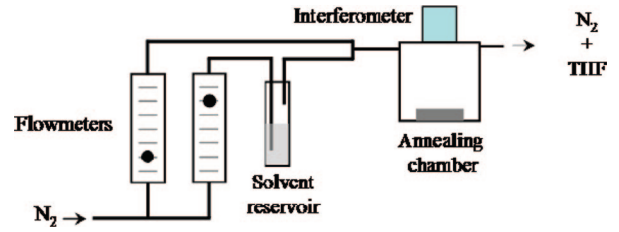

Figure 1. Schematic diagram of experimental setup used for solvent annealing.

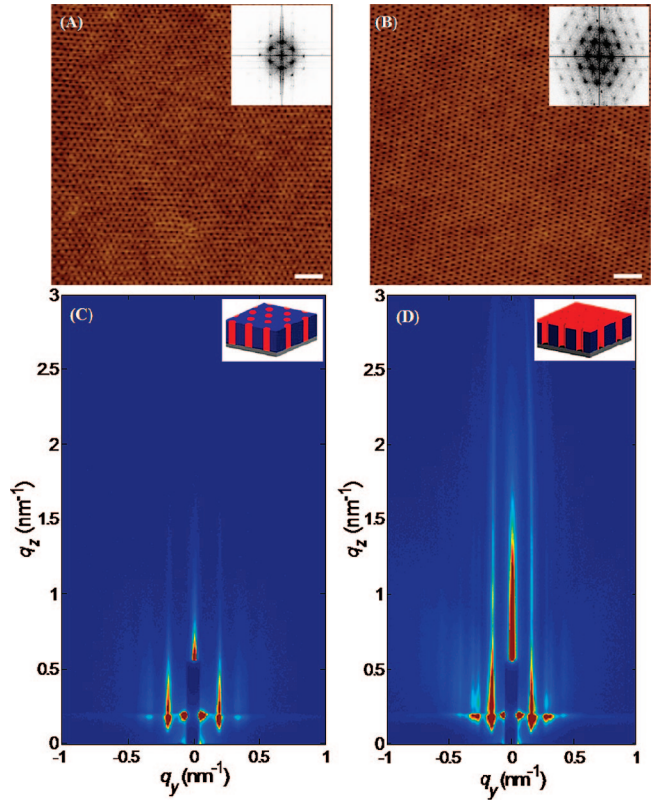

Figure 2. Height mode SFM images of highly ordered PS-*b*-P4VP films to silicon. (A) Solvent annealed films. (B) Surface reconstruction of the ordered films. The impressive degree of order is reflected in the Fourier transform, as shown in the inset. Schematic illustration of solvent annealed and reconstructed films was shown in the right-hand side. Scale bar is 200 nm.

Nanoscope III) in the tapping mode. The measurements were performed using commercial Si cantilevers. The film thickness was measured by ellipsometry. To characterize the structure of spin-coated and solvent annealed PS-*b*-P4VP thin films, grazing incidence small-angle X-ray scattering (GISAXS) measurements were performed at beamline X22B (National Synchrotron Light Source, Brookhaven National Laboratory) using X-rays with a wavelength of $\lambda = 1.525$ Å. The exposure time was 15 s per frame.

Results and Discussion

The simple process of solvent evaporation can produce highly ordered arrays of cylindrical microdomains oriented normal to the surface in block copolymers with long-range lateral order. Solvent evaporation presents a simple route not only in controlling the alignment of the microdomain morphology, but also in enhancing the lateral order of microdomains in BCP thin films. Figure 2 shows scanning force microscopic (SFM) images and schematic diagram of solvent-annealed and surface-reconstructed PS-*b*-P4VP films on a silicon substrate with a native oxide layer. Highly ordered arrays of cylindrical micro-

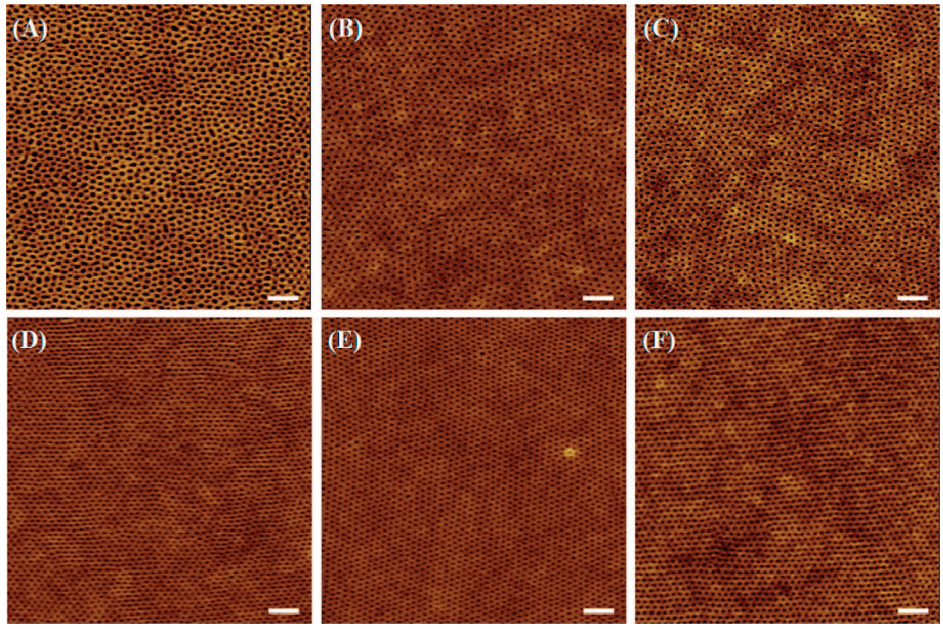

Figure 3. Time evolution of surface morphologies of reconstructed PS-*b*-P4VP films developed under THF vapor at different times (Height mode SFM images). (A) As-spun, (B) 30 min, (C) 1 h, (D) 2 h, (E) 3 h, and (F) 4 h. As the annealing time increases, the lateral ordering is significantly enhanced. Scale bar is 200 nm.

domains oriented normal to the surface were obtained during solvent annealing in THF vapor for 3 h (Figure 2A).

Solvent annealing was performed in THF vapor for 3 h under N_2 environment at 23 °C. When the solvent annealed films were immersed in ethanol, a good solvent for P4VP and a nonsolvent for PS, a reconstruction of the film was observed where highly ordered arrays of nanoscopic pores were formed (Figure 2B). Surface reconstruction is a process where, upon exposure of the BCP film to a solvent that is a good solvent for the minor component block and a nonsolvent for the major component block, the minor component is drawn to the surface of the film, and, upon drying, cylindrical nanopores are produced with dimensions comparable to the original cylindrical microdomains. The surface of the film is also covered with the minor component block. The reconstruction of the film maintains the well-developed microdomain structure and the sharpened distribution of size and center-to-center distance between the nanoscopic pores, as in the solvent annealed films.[32,34] The thickness of the solvent annealed and reconstructed PS-*b*-P4VP films were 29.5 and 33.3 nm, respectively, as measured by ellipsometry. The Fourier transforms of the SFM images are shown in the insets of Figure 2A and B. Six-point patterns, with multiple higher-order reflections, are seen, which is characteristic of a long-range lateral ordering. It should be noted that reconstruction method can be used to generate nanoscopic pores without removal of the minor component block by chemical or photolytic degradation, as is the case with some other BCPs.[36−38] In addition, the BCP after exposure to the preferential solvent is unchanged. Because the glass transition of the PS is well above room temperature, the nanopores are maintained since the PS matrix is glassy. From SFM images of solvent annealed and reconstructed PS-*b*-P4VP films, it is difficult to distinguish between the two components. After the reconstructed film was floated on a HF buffer (1 wt %) solution, it was transferred onto a silicon substrate so that both the top and the bottom of the film could be examined, as reported previously.[34] The nanopores were found to span across the entire film. In addition, grazing incidence small-angle X-ray scattering (GISAXS) was used to investigate both the solvent annealed and reconstructed films. Figure 2C shows the GISAXS of a solvent annealed film where Bragg rods (reflections extended along q_z), characteristic of P4VP cylindrical microdomains oriented normal to the film surface, are seen. as evidenced by the extension of the scattering along q_z direction. The GISAXS pattern of the reconstructed films show multiple-orders of Bragg rods, due to the enhanced contrast in the film arising from the significant increase in the contrast (Figure 2D).

The time evolution of surface morphologies of PS-*b*-P4VP thin films under THF vapor was investigated. An interferometer was used to measure the thickness of the film during solvent annealing. The film thickness was examined by varying the degree of swelling on a 29.4 nm thick as-spun film as a function of annealing time. The average thickness of swollen films at each annealing time (30 min, 1, 2, 3, and 4 h) was 35.1, 42.2, 44.3, 44.5, and 44.5 nm, respectively. It should be noted that thickness of swollen film reaches a saturation point after solvent annealing for 2 h. Figure 3 shows the SFM images of reconstructed films at different annealing times. The SFM image of the spin-coated film (Figure 3A) shows a surface covered with circular domains, having an average separation distance of 50.8 ± 12.9 nm and an average diameter of 35.4 ± 8.3 nm as shown in Figure 4.

Upon exposure to the THF vapors, a slightly selective solvent for PS block, under N_2 for 30 min, a hexagonal array of the cylindrical microdomains with a slightly enhanced lateral ordering and narrower domain size distribution were obtained (Figure 3B). The films annealed for 30 min show an average microdomain separation distance of 48.3 ± 7.3 nm and an average microdomain diameter of 27.2 ± 5.6 nm as shown in Figure 4 from an image analysis. When the annealing time was increased to 1 h, arrays of the cylindrical microdomains with a significantly enhanced lateral ordering and much narrower domain size distribution were obtained as shown in Figure 3C. Over 2 × 2 μm^2 areas, distribution in domain size and average separation distance, as shown in Figure 3D−F and Figure 4, did not change significantly with further exposure to solvent. Therefore, the characterization of the annealed films over larger areas was required.

Moiré pattern analyses were used to characterize the orientation, grain size, and dislocations of cylindrical microdomains

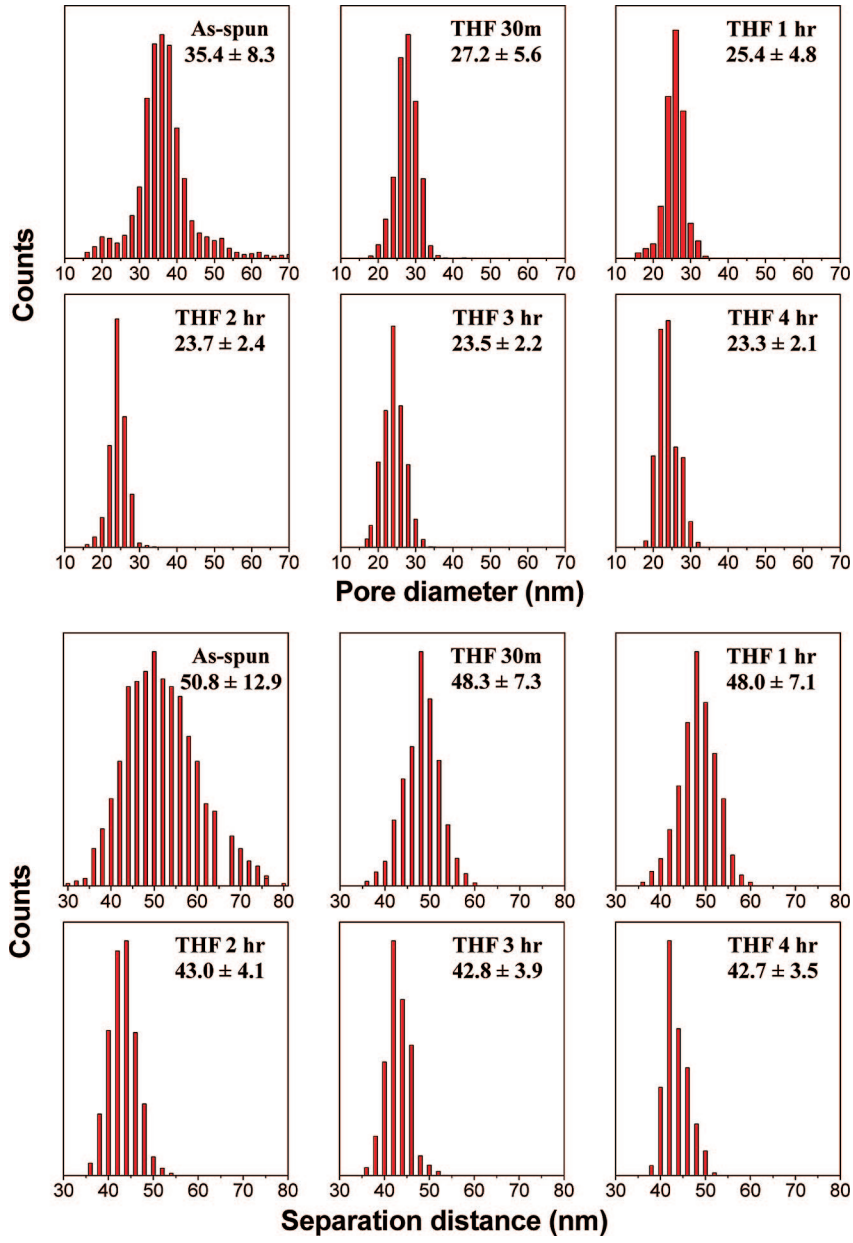

Figure 4. Image analyses of PS-*b*-P4VP films developed at different annealing times. (A) Distribution of average pore diameter. (B) Distribution of average center-to-center distance of pores. After solvent annealing for 2 h, much narrower distribution was obtained.

over large areas.[39,40] Moiré patterns are formed from interferences between a reference and a sample grating. Under certain conditions, grain size, shape, orientation, and dislocations can be seen directly. Figure 5 shows Moiré patterns of PS-*b*-P4VP films measured in the phase mode using SFM with scan angle of 10 degrees at four different annealing times. As the annealing time increases, the grain size of the cylindrical microdomains increased, as shown in Figure 5. The films annealed for 4 h show a large single $10 \times 10\ \mu m^2$ grain with only a few dislocation points. In the case of film annealed for 30 min, small grain of hundreds of nanometer was observed in the same scan areas (not shown here).

To further characterize the two-dimensional (2-D) ordering of the PS-*b*-P4VP film as a function of solvent annealing time, the orientation correlation function was used. The orientational correlation function is defined as[41]

$$G_6(r) = <\phi_6^*(0)\phi_6(r)> \quad (1)$$

where

$$\phi_6(r_j) = \frac{\sum_{j=1}^{NN} \exp(6i\theta(r_{ij}))}{NN} \quad (2)$$

and $\varphi_6^*(0)$ indicates the complex conjugate of the order parameter of the cylindrical microdomains which is designated as the origin, index j counts the nearest-neighbors, NN, of cylinder i and $\theta(r_{ij})$ is the angle made between the bond connecting cylinders i and j and an arbitrarily chosen reference axis. Each cylinder is used as the origin for one calculation, and the angular brackets indicate an average over all cylinders. $G_6(r)$ has a value between 0 and 1 for all r. For a perfect hexagonal crystal, a plot of $G_6(r)$ versus r will have a value of 1 and will only exist when $r = na$, where n has a integer value. In a real crystal, the maximum value of this graph will not be 1.0 due to fluctuations in lattice positions even for a well-ordered 2-D crystal.

Figure 6 shows the orientational correlation function calculated from SFM images of as-spun and solvent annealed PS-*b*-P4VP in Figure 3. For clarity the orientational order parameter calculated for each film was displaced along the *y*-axis. The

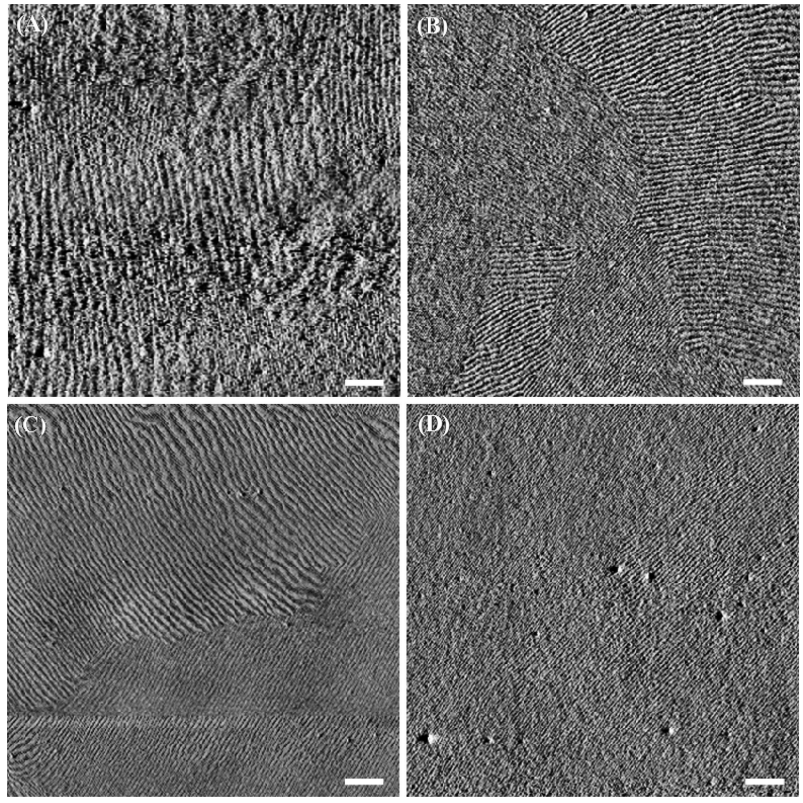

Figure 5. Moiré analysis of solvent annealed PS-*b*-P4VP films measured from phase mode SFM scan. Moiré pattern of the films annealed for (A) 1 h, (B) 2 h, (C) 3 h, and (D) 4 h was seen. As the annealing time increases, the grain size of cylindrical microdomains also increases. Scale bar is 1 μm.

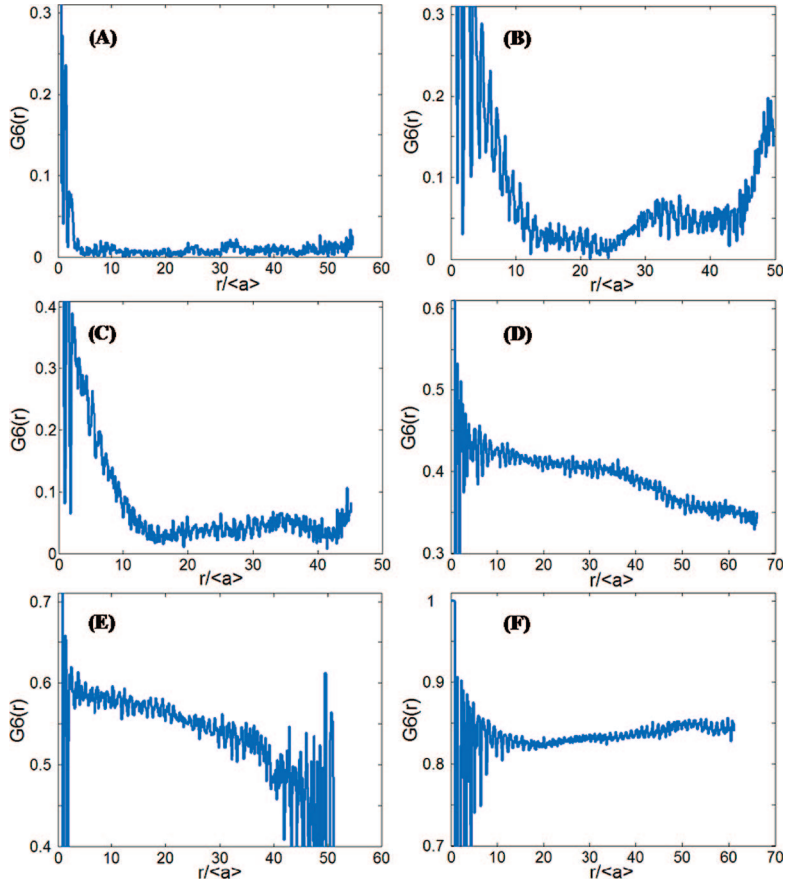

Figure 6. Orientational correlation function calculated from various solvent annealed PS-*b*-P4VP samples. The orientational order of the films developed at (A) as-spun, (B) 30 min, (C) 1 h, (D) 2 h, (E) 3 h, and (F) 4 h was seen. The local orientational order was significantly enhanced with longer annealing time.

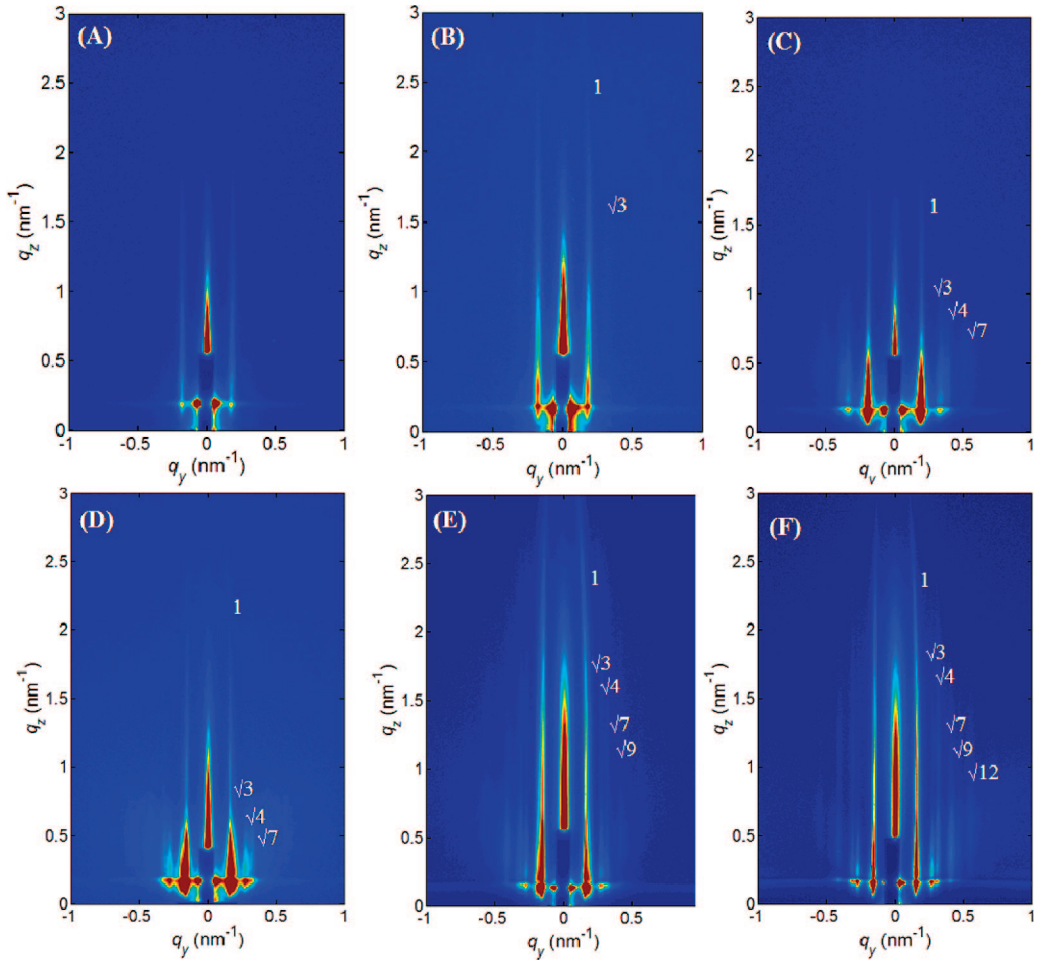

Figure 7. GISAXS patterns of PS-b-P4VP films developed at six different annealing times: (A) as-spun, (B) 30 min, (C) 1 h, (D) 2 h, (E) 3 h, and (F) 4 h. The films annealed over 2 h exhibit higher order scattering peaks along with q_y axis. Six different samples were measured above the critical angle ($\alpha = 0.20°$) of polymer ($\alpha = 0.16°$).

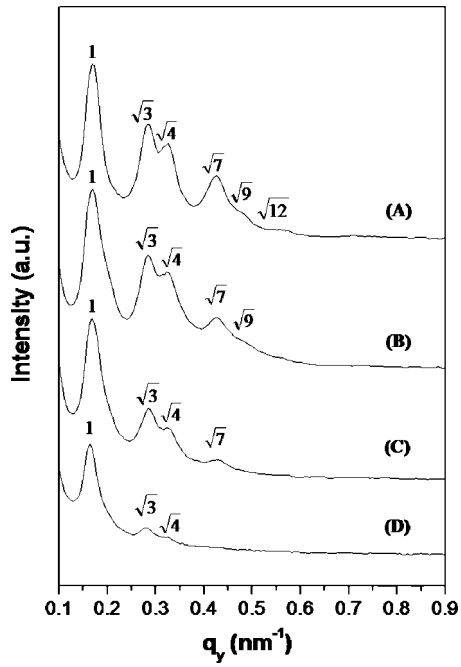

Figure 8. Detailed line scans along q_y of the films annealed for (A) 4 h, (B) 3 h, (C) 2 h, and (D) 1 h. Lateral ordering of each annealed films was seen much clearly from detailed line scans.

local orientation order parameter calculated from as-spun and the film annealed for short time (~30 min) is extremely close to 0, the value of randomly oriented lattice. As the annealing time increases, the orientational order parameter gradually increases, as shown in Figure 6. In the case of a film annealed for 4 h, the local orientational order parameter is 0.85, which is close to 1, the value of a perfect lattice. $G_6(r)$ decays very little over large distances, which implies the presence of long-range orientational order.

Moiré analysis from SFM can characterize the local structure of BCP thin films on the tens of micrometers size scale. To characterize the structures of these thin films over a much larger areas, grazing incidence small-angle X-ray scattering (GISAXS) was used to characterize the orientation and lateral ordering of the morphology in the thin films. To enhance the electron density difference between the matrix and nanoscopic elements, the reconstruction process was used for six different samples. Figure 7 shows the GISAXS patterns of six different BCP thin films measured above the critical angle ($\alpha = 0.20°$) of polymer ($\alpha_c = 0.16°$). When the incidence angle was set, above the critical angle of the polymer (0.16°) but below the critical angle for Si (0.22°), the X-rays penetrate into the polymer film and are totally reflected at the Si interface, enhancing the scattering observed for the polymer film. All GISAXS patterns show that the PS-*b*-P4VP cylindrical microdomains are oriented normal to the film surface, as evidenced by the extension of the scattering along q_z. As the solvent annealing time increases, multiple higher order reflections are seen, as shown in Figure 7.

Detailed line scans along q_y at $q_z = 0.19$ nm^{-1} of BCP thin films annealed in THF vapors for 1, 2, 3, and 4 h are shown in Figure 8. Here q_y is the momentum transfer normal to the incident plane (i.e., parallel to the film surface), while q_z is normal to the sample surface. Figure 8A shows that the relative scattering vectors (q_y) of the six peaks are $1:\sqrt{3}:\sqrt{4}:\sqrt{7}:\sqrt{9}:\sqrt{12}$, indicating that hexagonal arrays of cylindrical microdomains with long-range lateral order developed in the films. The first order peak was observed at $q_y = 0.171$ nm^{-1}, which corresponds to a center-to-center distance between the microdomains of 42.4 nm. This spacing is consistent with the result obtained from SFM measurements. With decreasing solvent annealing times the higher order reflections disappear, as shown in Figure 8B−D. These results are consistent with the results from the Moiré analysis of the SFM images.

Conclusions

Thin films of PS-*b*-P4VP BCPs having a cylindrical microdomain morphology were annealed in THF vapor, a slightly selective solvent for PS block to enhance the orientation and lateral ordering of the microdomains. The orientation, lateral ordering, and grain size of the cylindrical microdomains were characterized by SFM, Moiré analysis, and GISAXS. As solvent annealing time increases, the lateral ordering of cylindrical microdomains is significantly enhanced, generating, ultimately, a single grain 10×10 μm^2 in size. The solvent annealing process, in combination with exposure to a solvent that preferentially solvates the minor component block, provides a simple approach to fabricate highly ordered nanoporous templates for pattern transfer to the underlying substrates or scaffolds for inorganic nanostructures.

Acknowledgment. This work was supported by the U.S. Department of Energy (DOE), the NSF supported MRSEC, and NSEC at the University of Massachusetts Amherst. Use of the National Synchrotron Light Source, Brookhaven National Laboratory, was supported by the U.S. Department of Energy, Office of Science, Office of Basic Energy Sciences, under Contract No. DE-AC02-98CH10886 through the Division of Materials Science.

References and Notes

(1) Hamley, I. W. *The Physics of Block Copolymers*; Oxford University Press: New York, 1998.
(2) Hadjichristidis, N.; Pispas, S.; Floudas, G. *Block Copolymers: Synthetic Strategies, Physical Properties, and Applications*; John Wiley & Sons: New York, 2002.
(3) Bates, F. S.; Fredrickson, G. H. *Annu. Rev. Phys. Chem.* **1990**, *41*, 525–557.
(4) Bates, F. S.; Fredrickson, G. H. *Phys. Today* **1999**, *52*, 32–38.
(5) Lodge, T. P. *Macromol. Chem. Phys.* **2003**, *204*, 265–273.
(6) Ruzette, A.-V.; Leibler, L. *Nat. Mater.* **2005**, *4*, 19–31.
(7) Segalman, R. A. *Mater. Sci. Eng.* **2005**, *R48*, 191–226.
(8) Li, M.; Ober, C. K. *Mater. Today* **2006**, *9*, 30–39.
(9) Hawker, C. J.; Russell, T. P. *MRS Bull.* **2005**, *30*, 952–966.
(10) Li, M.; Coenjarts, C. A.; Ober, C. K. *Adv. Polym. Sci.* **2005**, *190*, 183–226.
(11) Pelletier, V.; Asakawa, K.; Wu, M.; Adamson, D. H.; Register, R. A.; Chaikin, P. M. *Appl. Phys. Lett.* **2006**, *88*, 211114.
(12) Black, C. T. *IEEE Trans. Nanotechnol.* **2004**, *3*, 412–415.
(13) Ross, C. A. *Annu. Rev. Mater. Res.* **2001**, *31*, 203–235.
(14) Maier, S. A.; Brongersma, M. L.; Kik, P. G.; Meltzer, S.; Requicha, A. A. G.; Atwater, H. A. *Adv. Mater.* **2001**, *13*, 1501–1505.
(15) Kim, D. H.; Lau, K. H. A.; Robertson, J. W. F.; Lee, O.-J.; Jeong, U.; Lee, J. I.; Hawker, C. J.; Russell, T. P.; Kim, J. K.; Knoll, W. *Adv. Mater.* **2005**, *17*, 2442–2446.
(16) Thurn-Albrecht, T.; DeRouchey, J.; Russell, T. P. *Macromolecules* **2000**, *33*, 3250–3253.
(17) Villar, M. A.; Rueda, D. R.; Ania, F.; Thomas, E. L. *Polymer* **2002**, *43*, 5139–5145.
(18) Bodycomb, J.; Funaki, Y.; Kimishima, K.; Hashimoto, T. *Macromolecules* **1999**, *32*, 2075–2077.
(19) Segalman, R. A.; Yokoyama, H.; Kramer, E. J. *Adv. Mater.* **2001**, *13*, 1152–1155.
(20) Stoykovich, M. P.; Müller, M.; Kim, S. O.; Solak, H. H.; Edwards, E. W.; de Pablo, J. J.; Nealey, P. F. *Science* **2005**, *308*, 1442–1446.
(21) Mansky, P.; Liu, Y.; Huang, E.; Russell, T. P.; Hawker, C. J. *Science* **1997**, *275*, 1458–1460.
(22) Drockenmuller, E.; Li, L. Y. T.; Ryu, D. Y.; Harth, E.; Russell, T. P.; Kim, H. C.; Hawker, C. J. *J. Polym. Sci., Part A: Polym. Chem.* **2005**, *43*, 1028–1037.
(23) Tang, C.; Tracz, A.; Kruk, M.; Zhang, R.; Smilgies, D.-M.; Matyjaszewski, K.; Kowalewski, T. *J. Am. Chem. Soc.* **2005**, *127*, 6918–6919.
(24) Morikawa, Y.; Nagano, S.; Watanabe, K.; Kamata, K.; Iyoda, T.; Seki, T. *Adv. Mater.* **2006**, *18*, 883–886.
(25) Kim, G.; Libera, M. *Macromolecules* **1998**, *31*, 2569–2577.
(26) Lin, Z.; Kim, D. H.; Wu, X.; Boosahda, L.; Stone, D.; LaRose, L.; Russell, T. P. *Adv. Mater.* **2002**, *14*, 1373–1376.
(27) Ho, R.-M.; Tseng, W.-H.; Fan, H.-W.; Chiang, Y.-W.; Lin, C.-C.; Ko, B.-T.; Huang, B.-H. *Polymer* **2005**, *46*, 9362–9377.
(28) Hahm, J.; Sibener, S. J. *Langmuir* **2000**, *16*, 4766–4769.
(29) Kimura, M.; Misner, M. J.; Xu, T.; Kim, S. H.; Russell, T. P. *Langmuir* **2003**, *19*, 9910–9913.
(30) Ludwigs, S.; Böker, A.; Voronov, A.; Rehse, N.; Magerle, R.; Krausch, G. *Nat. Mater.* **2003**, *2*, 744–747.
(31) Kim, S. H.; Misner, M. J.; Xu, T.; Kimura, M.; Russell, T. P. *Adv. Mater.* **2004**, *16*, 226–231.
(32) Park, S.; Kim, B.; Wang, J.-Y.; Russell, T. P. *Adv. Mater.* **2008**, *20*, 681–685.
(33) Martin, T. M.; Young, D. M. *Polymer* **2003**, *44*, 4747–4754.
(34) Park, S.; Wang, J.-Y.; Kim, B.; Chen, W.; Russell, T. P. *Macromolecules* **2007**, *40*, 9059–9063.
(35) Xu, T.; Stevens, J.; Villa, J.; Goldbach, J. T.; Guarini, K. W.; Black, C. T.; Hawker, C. J.; Russell, T. P. *Adv. Funct. Mater.* **2003**, *13*, 698–702.
(36) Thurn-Albrecht, T.; Schotter, J.; Kästle, G. A.; Emley, N.; Shibauchi, T.; Krusin-Elbaum, L.; Guarini, K.; Black, C. T.; Tuominen, M. T.; Russell, T. P. *Science* **2000**, *290*, 2126–2129.
(37) Mao, H.; Hillymyer, M. A. *Soft Matter* **2006**, *2*, 57–59.
(38) Du, P.; Li, M.; Douki, K.; Li, X.; Garcia, C. B. W.; Jain, A.; Smilgies, D.-M.; Fetters, L. J.; Gruner, S. M.; Wiesner, U.; Ober, C. K. *Adv. Mater.* **2004**, *16*, 953–957.
(39) Pashley, D. W.; Menter, J. W.; Basset, G. A. *Nature (London)* **1957**, *179*, 752–755.
(40) Hexemer, A.; Stein, G. E.; Kramer, E. J.; Magonov, S. *Macromolecules* **2005**, *38*, 7083–7089.
(41) Segalman, R. A.; Hexemer, A.; Hayward, R. C.; Kramer, E. J. *Macromolecules* **2003**, *36*, 3272–3288.

MA802480S